ULTRA-HIGH REJECTION OPTICAL FILTERS

Dr. T. M. Shay

Shay Aerospace Corp
1300-G El Paseo #304
Las Cruces, NM 88001
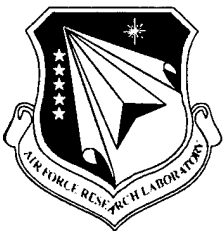
13 June 1998

Final Report

19981118 005

APPROVED FOR PUBLIC RELEASE; DISTRIBUTION IS UNLIMITED.

DTIC QUALITY INSPECTED

AIR FORCE RESEARCH LABORATORY
Directed Energy Directorate
3550 Aberdeen Ave SE
AIR FORCE MATERIEL COMMAND
KIRTLAND AIR FORCE BASE, NM 87117-5776

AFRL-DE-PS-TR-1998-1056

Using Government drawings, specifications, or other data included in this document for any purpose other than Government procurement does not in any way obligate the U.S. Government. The fact that the Government formulated or supplied the drawings, specifications, or other data, does not license the holder or any other person or corporation; or convey any rights or permission to manufacture, use, or sell any patented invention that may relate to them.

This report has been reviewed by the Public Affairs Office and is releasable to the National Technical Information Service (NTIS). At NTIS, it will be available to the general public, including foreign nationals.
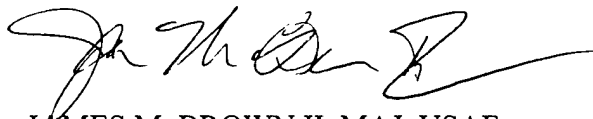
If you change your address, wish to be removed from this mailing list, or your organization no longer employs the addressee, please notify AFRL/DE, 3550 Aberdeen Ave SE, Kirtland AFB, NM 87117–5776.

Do not return copies of this report unless contractual obligations or notice on a specific document requires its return.

This report has been approved for publication.

PAUL D. HILLMAN
Project Manager

FOR THE COMMANDER

JAMES M. BROWN II, MAJ, USAF
Acting Chief, Starfire Optical Range Division

R. EARL GOOD, SES
Director, Directed Energy Directorate

REPORT DOCUMENTATION PAGE

Form Approved
OMB No. 074-0188

Public reporting burden for this collection of information is estimated to average 1 hour per response, including the time for reviewing instructions, searching existing data sources, gathering and maintaining the data needed, and completing and reviewing this collection of information. Send comments regarding this burden estimate or any other aspect of this collection of information, including suggestions for reducing this burden to Washington Headquarters Services, Directorate for Information Operations and Reports, 1215 Jefferson Davis Highway, Suite 1204, Arlington, VA 22202-4302, and to the Office of Management and Budget, Paperwork Reduction Project (0704-0188), Washington, DC 20503

1. AGENCY USE ONLY (Leave blank)	2. REPORT DATE 13 Jun 98	3. REPORT TYPE AND DATES COVERED Final, 1995- 1998

4. TITLE AND SUBTITLE
Ultra-High Rejection Optical Filters

5. FUNDING NUMBERS

C: F29601-95-C-0162
PE: 65502F

6. AUTHOR(S)

Dr. T. M. Shay

PR: 3005
TA: C0
WU: JS

7. PERFORMING ORGANIZATION NAME(S) AND ADDRESS(ES)

Shay Aerospace Corp
1300-G El Paseo, #304
Las Cruces, NM 88001

8. PERFORMING ORGANIZATION REPORT NUMBER

9. SPONSORING / MONITORING AGENCY NAME(S) AND ADDRESS(ES)

Air Force Research Laboratory/DES
3550 Aberdeen Ave SE
Kirtland AFB, NM 87117

10. SPONSORING / MONITORING AGENCY REPORT NUMBER

AFRL-DE-PS-TR-1998-1056

11. SUPPLEMENTARY NOTES

12a. DISTRIBUTION / AVAILABILITY STATEMENT
Approved for public release; distribution is unlimited.

12b. DISTRIBUTION CODE

13. ABSTRACT (Maximum 200 Words)
We developed a theoretical model for a novel optical filter called the Laser Induced Optical Filter (LIDOF). The model showed that a 500-W power pump laser should be able to pump the LIDOF hard enough to generate a signal throughput of 80%. A custom pulsed dye laser pump has been built, tested, and delivered. This pump laser has a 0.07 cm^{-1} linewidth and an output power of 3.6 kW; the LIDOF requires a linewidth of < 0.1 cm^{-1} and a pump power of 500 W. Thus, our pump laser exceeds the requirements of the LIDOF. In addition, the LIDOF head, including the Na2 heat pipe, the polarizers, the photo-detectors, and the pump and signal separating optics, have all been designed, assembled, and tested. The hardware for the testing of this filter has been delivered. The final LIDOF testing was not completed due to the lack of a suitable test source. We also designed, built, and delivered a working Faraday anomalous dispersion optical filter that operates at the Na D$_2$ line. This filter was tested using an Air Force Research Laboratory test oscillator and the Na filter met specifications.

14. SUBJECT TERMS
Narrow Band Pass Filter, Molecular Filter, Laser Induced Optical Filter

15. NUMBER OF PAGES
28

16. PRICE CODE

17. SECURITY CLASSIFICATION OF REPORT	18. SECURITY CLASSIFICATION OF THIS PAGE	19. SECURITY CLASSIFICATION OF ABSTRACT	20. LIMITATION OF ABSTRACT
Unclassified	Unclassified	Unclassified	Unlimited

NSN 7540-01-280-5500

i

Standard Form 298 (Rev. 2-89)
Prescribed by ANSI Std. Z39-18
298-102

Table of Contents

ILLUSTRATIONS

TABLES

SUMMARY REPORT

1) Purpose of the work:

    To develop ultra-high background rejection optical filters for the Starfire Optical Range beacon laser that will allow 24-hour operation of the adaptive optics.

2) Description of the work carried out:

    We developed a theoretical model for an novel optical filter called the Laser Induced Optical Filter. The hardware for the testing of this filter has been designed and delivered. All that remains is the testing of the filter with a suitable source. We designed, built and delivered a working FADOF ultra-high background rejection optical filter that operates at the Na D_2 line.

3) Results:

    The model has shown that the LIDOF concept is feasible at 532 nm. The LIDOF hardware has been delivered. A Na FADOF was delivered and was tested at SOR to have a background rejection of 2 10^{-6} and a throughput of ~ 80%.

4) Potential Applications:

    The Na FADOF can be applied at SOR for Na line laser beacons. This device reduces the background line entering the system by a factor of 2 10^{-6} and it offers a high transmission. Thus it is applicable to any active imaging or remote sensing application that can be operated at a strong alkali atom transition. These devices have been used to monitor welding in real time, which might be applicable in manufacturing applications.

1)   Introduction

In the existing adaptive optical atmospheric compensation system, frequency doubled Nd:YAG lasers are used to transmit laser beacon pulse into the atmosphere. The beacon signal generated by the laser pulse back-scattered from the atmosphere is used to compensate for the atmospheric wavefront distortions. However, this beacon is very weak and, in current adaptive optical systems, the optical noise from the bright skylight swamps the very weak beacon signal during daylight hours. Therefore, the current adaptive optical systems can only operate at night when the skylight levels have been reduced by more than 6 orders of magnitude. Conventional optical filters have inadequate throughput and out-of-band rejection for this system. We modeled and assembled a high transmission, ultra-high rejection optical filter for frequency doubled Nd:YAG laser lines that will provide sufficient skylight suppression so that the adaptive optical system can be operated during the daytime. The filter system can be gated by tuning the pump on and off. The gating is desirable for two reasons: First, the beacon signal is sensed only over a small "range gate" in the atmosphere. So isolating the range gate is accomplished only by turning the filter on for a short time. Second, it is possible to only turn the filter on after the laser beam leaves the telescope so that the light scattered by the telescope optics as the pulsed laser beam leaves the telescope does not saturate the wavefront sensor. The gated filter should have rise and fall times of roughly 25 ns.

In Phase II we designed, built, and delivered a high throughput, ultra-high background rejection optical filter short pulse gatable system for the Nd:YAG laser lines. The Phase I feasibility study showed that a throughput of greater than 80% and solar background rejection of greater than 10^5 can be built using the Na_2 Light Induced Dispersion Optical Filter, LIDOF. This LIDOF will also have a 25 ns risetime. For time durations longer than 50 ns the LIDOF temporal response should follow the pump pulse temporal characteristics. Thus, the LIDOF provides an optical filter whose temporal response is easily tailored by changing the pump pulse duration. The LIDOF will enable the atmospheric wavefront compensation system to operate in bright daylight. In addition, the success of this filter will open the commercial application for many laser wavelengths in the area of lidar, or ladar, freespace laser communications, etc., where the solar radiation usually severely degrade the optical instrument performance.

We modeled, designed, and built an ultra-high background rejection Na_2 LIDOF and fast gating system for Na vapor laser lines at wavelengths of 532-nm. The Na_2 vapor has a number of transition wavelengths that match the frequency doubled Nd:YAG laser line. The operating temperature ranges from 500 °C to 600 °C depending upon the filter transition used. The following sub-sections will provide an explicit, detailed description of the Phase II effort. They include theory, LIDOF hardware, and design.

2) Filter Approach and Theory

To build an optical filter based on the atomic or molecular transitions, one must find suitable atomic or molecular transitions that satisfy the following basic requirements: (1) atomic/molecular transition wavelengths that match the signal wavelengths; (2)

adequate atomic/molecular vapor pressure that exits within a practical temperature range; (3) sufficient large absorption cross section at the filter transitions. In addition, the thermal noise that is generated by the vapor oven must not cause appreciable noise at the photodetector. In the next section this is analyzed in detail.

(A) Filter Photon Noise Generated by a Black Body Radiator

At visible and infrared wavelengths the black body radiation of objects can sometimes be a significant internal noise source in a hot filter and can lead to a degradation in filter performance. To systematically estimate the effects of the black body radiation, we have developed a model for calculating the noise equivalent power, NEP for a generic filter configuration. That model is discussed in this section.
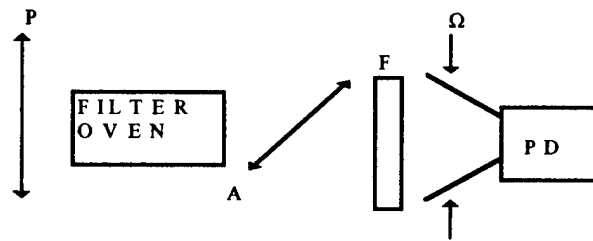

Fig. 1. The generic filter system.

The generic filter system we are considering is shown in Fig. 1. In Fig. 1, P and A are the polarizer and analyzer. An optical filter, F, is used to limit the spectral band of the black body radiation that reaches the photo-detector, PD, while transmitting the signal wavelength. Ω is the field-of-view of the photo-detector. The photo-detector has an active area of A and a quantum efficiency of η for the signal wavelength.

The noise equivalent power, NEP, of the optical filter system depends upon the shot noise generated by the black body radiation photon that reaches the photo-detector. Hence,

$$NEP = \left(\frac{P_{BBD} * BW * hc}{\eta * \lambda_s} \right) , \qquad \text{Eq. 1}$$

where P_{BBD} represents the oven black body power that is incident upon the photo-detector's active area, and BW represents the photo-receiver systems electronic bandwidth. For an ideal interference filter with a passband of $\Delta\lambda_F$,

$$P_{BBD} = L_{e\lambda}(\lambda_s, T) \cdot \Delta\lambda_F \cdot \Omega \cdot A_{OVEN} \cdot \eta_{OVEN} \cdot T_F \cdot T_A$$

$$\text{Eq. 2}$$

where $L_{e\lambda}$ (λ_s, T) represents the spectral irradiance of an ideal black body radiator at temperature T, A_{oven} represents the oven surface area, and ε_{oven} represents the emissivity of the oven. T_F and T_A represent the optical filter and analyzer transmissions, respectively. Clearly, if you must operate at a given temperature T, wavelength λ_s, and A_{oven}, then, in general, you want to decrease $\Delta\lambda_F$ and λ_s so that there is less black body

radiation reaching the photodetector. Eqs. 1 and 2 can be used to calculate the NEP of the system that is due to the filter's black body radiation. We will assume that a noise equivalent power of between $2pW/(Hz)^{1/2}$ and $30\ fw/(Hz)^{1/2}$ are acceptable since these correspond to the noise equivalent powers of good low noise PIN and avalanche photodiode receivers, respectively.

We will assume that the system is configured to minimize P_{BBD}. For the purpose of estimating the noise equivalent power, we have assumed the values in Table I. The optical filter chosen is the BG-40 color glass filter that will be used in the LIDOF. The solid angle listed corresponds a field-of-view of $\pm 5°$. The detector efficiency corresponds to the efficiency of a silicon photodiode at 500-nm.

Table I. Black body radiator noise parameters

$\Delta\lambda_F$	250 nm
T_F	0.86
A_{oven}	π x 1 in x 3 in
$\delta\Omega$	23.9×10^{-3} sr
ε_{oven}	1
η	0.4

We can now calculate an upper limit on the oven operating temperature for a given material if we have a maximum allowable noise equivalent power, NEP_{max}. We choose a somewhat arbitrarily a noise equivalent power,

$$NEP_{max} = \frac{2\ pW}{\sqrt{Hz}} \qquad \text{Eq. 3}$$

The spectral irradiance of an ideal black body radiator at a temperature T,

$$L_{e\lambda}(\lambda_s, T) = \frac{2 * h * c^2}{\lambda_s^5 * (Exp[h * c / (k * T * \lambda_s)] - 1)}, \qquad \text{Eq. 4}$$

where h and k represents Plank's and Boltzman's constants, c represents the speed of light, and λs represents the signal wavelength. Now Eq. 4 and 2 can be combined and substituted into the right hand side of Eq. 1 and set equal to Eq. 3 to obtain,

$$NEP_{max} = \frac{\sqrt{(L_{e\lambda} * \Omega * \Delta\lambda_F * T_A * T_F * A_{oven} * \varepsilon_{oven} * hc * BW)}}{\sqrt{(\lambda_s * \eta)}}. \qquad \text{Eq.5}$$

Table II lists the results of a numerical solution of Eq. 5 for several wavelengths of interest. As you can see, the temperature where the NEP is $2\ pW/(Hz)^{1/2}$ falls dramatically as the wavelength increases. This simple analysis provides us with a simple thumb rule for eliminating systems that operate at temperatures significantly higher than $TNEP_{max}$.

Table II. Maximum oven temperatures for a given noise equivalent power versus wavelength.

$\lambda(\mu m)$	$T(^{\circ}C)$ for $NEP_{max} = 2$ $pW/(Hz)^{1/2}$	$T(^{\circ}C)$ for $NEP_{max} = 30$ $fW/(Hz)^{1/2}$
0.5	1025	665
0.6	920	570
0.8	700	400
1.0	540	270
1.5	380	140
2.0	280	64
3.0	180	-20

Table II shows that excellent noise characteristics can be maintained at 500-nm as long as the oven temperature is maintained below 665 °C. The color filter transmission can be as high as 94% so there is a small trade off in using the interference filter.

The bottom line is that oven temperatures of up to 600 °C can be tolerated in a filter operating at 532-nm without degrading the signal to noise ratio of the detection process. Higher temperatures can be tolerated if the color glass filter is replaced by a narrower bandwidth interference filter. However, the interference filter transmissions are always lower than the color glass filters so this will usually degrade the signal to noise ratio.

(B) Previous Ultra-High Background Rejection Optical Filters

In the past, we have invented and developed Faraday anomalous dispersion optical filter (FADOF)[1-9] that use alkali vapors for high background rejection optical filters. The comparison of the FADOF with other types filters is shown in Table III.

Table III.   The Performance of Some Narrow Bandwidth Optical Filters

	Interference	Quartz Lyot	Atomic Resonance	FADOF
Throughput	0.5	0.2	0.1-0.5	>0.8
Noise Rejection Factor	20-30 dB	35 dB	40-60 dB	50-60 dB
Field-of- view	±2.5-30 °	±30 °	± 90 ° **	± 90 ° *
Bandwidth (nm)	2-20	0.33	.001-.01	.001-.005
Response Time (ns)	.00004-.0004	0.005	10-10000	.2-1
Imaging	yes	yes	no	yes

* The field-of-view is fundamentally ±90°. However, the field-of-view is limited to about 10° by geometrical considerations.

** The field-of-view of the atomic resonance filter is limited to ±20° by practical considerations.

The noise rejection factor (NRF) in Table III is defined as

$$NRF = \frac{(Total\,incident\,noise)\,T_{max}}{Total\,noise\,transmitted} \qquad , \qquad \text{Eq. 6}$$

where T_{max} is the peak transmission of the filter. The higher the NRF, the better the background rejection. The wide FOV and excellent image preserving characteristics make the FADOF useful for wavefront sensing and imaging applications. The interference filter represents conventional technology and is inexpensive, but it has a wide bandpass and, hence, low NRF. The Lyot[10] filter has a moderate bandpass and moderate field-of-view, but does not meet the background rejection requirements for the application. The atomic resonance optical filter provides a narrow bandpass, wide field-of-view, and high background noise rejection.[11-15] However, these filters are not image preserving; furthermore they are very expensive to build. They, therefore, have limited usefulness in optical tracking. The FADOF is clearly advantageous to the other narrow bandwidth optical filters. In addition, the FADOF is insensitive to mechanical vibrations and misalignment.

We developed an optical filter that uses molecular vapors. Because of the high density of allowed transitions in molecules, there are several species that have transitions at the frequency doubled Nd:YAG laser wavelengths. The major difference between atomic and molecular species is that the vibration and rotational energy structure of the molecules gives rise to many more absorption lines than the atoms have. This is advantageous in terms of finding a filter wavelength to overlap the signal wavelength. However, because the thermal equilibrium population of the molecules is spread out over thousands of energy levels, the ratio of molecular population density on any one energy

level to the total molecular population is very low. Thus, the molecular density must be much higher than the vapor density of the atomic filter systems. Therefore, collisional broadening would be more severe in the molecular filter systems. Also, because there are many molecular transition lines close together, it would be difficult to distinguish the one signal transition from other transitions, this would mean a degradation of the background rejection of the filter. These facts force us to find a new concept for the building of a high background rejection optical filter.

The Light Induced Dispersive Optical Filter (LIDOF) is the concept which we developed in this effort. We proposed for the first time to use optical pumping for an ultra-high background rejection optical filter. Optical pumping has been used for simplifying complex molecular spectra. The spectroscopic method is called polarization labeling spectroscopy [13-17]. The optical pumping creates a non equilibrium population density in the Zeeman sublevels of the selected molecular state. Hence, a birefringence is generated in the vapor, but only for the molecular energy level that is pumped. Thus the molecular vapor only appears anisotropic for wavelengths that are absorbed by the lower energy level of the optically pumped energy level and for no others. Thus, if the birefringence and cell length are properly adjusted, a very narrow bandwidth $\pi/2$ polarization rotation is created, just as it is in the FADOF. In the LIDOF, the optical pumping field serves the same function as the magnetic field in the FADOF. They both orient the molecules. Fig. 2 shows the basic block diagram of the light-induced dispersion optical filter (LIDOF).
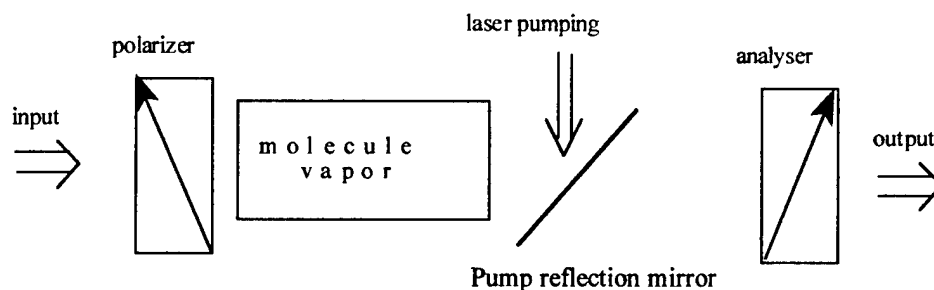

Fig. 2. The block diagram of the LIDOF.

A molecular vapor cell is placed between crossed polarizers and the birefringence is generated by optically pumping with a circularly polarized laser tuned to deplete a specific molecular ro-vibrational level. The pump wavelength may be selected to be far enough from the signal wavelength so that a simple color glass filter can be used prevent the pump radiation from reaching the detector.

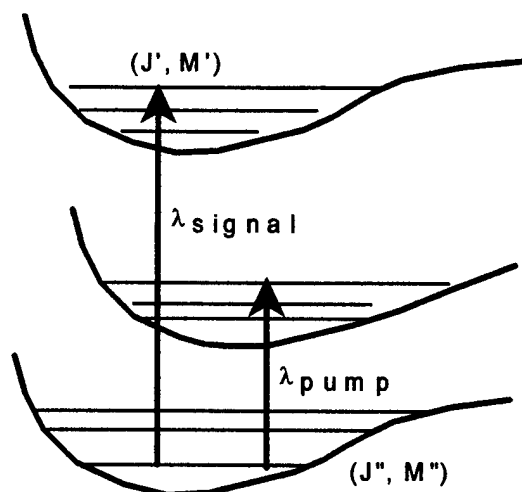Fig. 3 shows the energy structure for the pumping and signal transition.

Fig. 3. The energy structure for the pumping and signal transition for the filter.

The circularly polarized laser pumping beam creates non-equilibrium population density distribution in the magnetic sublevels of the (J", M") state. The pump transition lower level and the signal transition lower level are the same. Fig. 4 illustrates what happens when the right-hand circularly optical pumping is tuned to the transition between J"=2 and J'=1. It is obvious that, if the pumping is strong, then some of the M" sublevels (M" = -2, -1, 0) will be depleted by the circularly polarized pumping while the M" = 1 and 2 are not depleted at all. This creates an anisotropy in the molecular vapor.
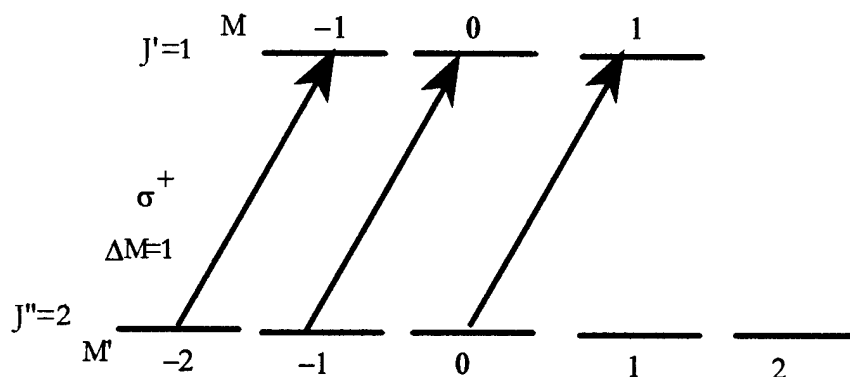

Fig. 4. An illustration of the circularly polarized pump creating non-equilibrium population distribution among the M" sublevels.

When the linearly polarized signal light is incident on the vapor cell, it can be decomposed into right-hand and left-hand circularly polarized components, a circularly birefringent material can therefore rotate the polarization of linearly polarized light. When a test signal is tuned close to a transition $(J'',M'')-(J',M')$, the two polarizations experience different refractive indices because of the non-equilibrium population of the level (J'', M'') created by pump beam. This results in optical rotation for the signal wavelength. Only the light whose wavelength is at the signal transition wavelength from level (J'', M'') will

experience optical rotation and pass through the crossed polarizer with high efficiency. Because of the optical transition selection rules, there are only three transitions allowed between rotational states in molecules.

To calculate the required pump power for the LIDOF, the Franck-Condon Factors for the transitions of interest must be known. In this case the Franck-Condon Factors were unknown. Therefore, we wrote a computer program to calculate them given the spectroscopic constants. This entailed a considerable effort and was completed. Given the FCF's and the fractional population in the lower level we were able to calculate the required pump intensity that ranged from 100 watts/cm^2 to 2 kW/cm^2.

To estimate the transmission of the LIDOF, we use the general transmission equation that is valid for any resonance birefringent medium placed between two crossed polarizers [2],

$$T(v) = \frac{1}{4}[e^{-\alpha_+(v)L} + e^{-\alpha_-(v)L} - 2Cos(2\theta(v))e^{-\frac{\alpha_-(v)+\alpha_+(v)}{2}L}] \qquad , \qquad \text{Eq. 7}$$

where $\pm$ denotes the left-handed and right-handed circular polarizations, v is the incident light frequency, L is the length of the vapor cell, $\alpha_\pm(v)$ is the absorption coefficient in the vapor cell, and $\theta(v)$ is the polarization rotation angle. The absorption coefficient can be calculated by

$$\alpha_\pm(v) = \sum_M n_M \sigma^\pm_{J''J'M}(v) \qquad , \qquad \text{Eq. 8}$$

where n_M is the molecular density on the magnetic sublevel of the groundstate level (v", J"), $\sigma^\pm_{J''J'M}(v)$ is the absorption cross-section for the transition (v',J',M$\pm$1)-(v",J",M) and can be derived as

$$\sigma^\pm_{J'J'M}(v) = \frac{3}{4}\frac{\lambda_0^2|\langle v'J'|v''J''\rangle|^2 g(v-v_0)}{\tau_{RAD}} \times \begin{cases} \dfrac{3(J\pm M+1)(J\pm M+2)}{(J+1)(2J+3)} & for J'=J''+1 \\[4mm] \dfrac{3(J\pm M+1)}{J(J+1)} & for J'=J'' \\[4mm] \dfrac{3(J\mp M)(J\mp M+1)}{J(2J-1)} & for J'=J''-1 \end{cases}$$

Eq. 9

where λ_0 is the transition wavelength, $|\langle v'J'|v''J''\rangle|^2$ is the Franck-Condon overlap factor for the transition (v'J'-v"J"). τ_{RAD} is the radiative lifetime of the level (v',J'). g(v-v$_0$) is the normalized line-shape function.

The polarization rotation angle, $\theta(\nu)$, is given by

$$\theta(\nu) = \frac{\pi \nu L}{c}[n_-(\nu) - n_+(\nu)] \quad ,$$

Eq. 10

where $n_\pm$ is the refractive index for the right-hand and left-hand circular polarizations, respectively. Using the Kramers-Kronig relations, we may calculate the refractive indices for circular polarizations

$$n^\pm(\nu) - 1 = \frac{c}{4\pi\nu} \frac{\mathrm{Im}[w(x+ib)]}{\mathrm{Re}[w(x+ib)]} \alpha^\pm(\nu) \quad ,$$

Eq. 11

where $w(x+ib)$ is the plasma dispersion function [18] and is given by

$$w(x+ib) = \frac{i}{\pi} \int_{-\infty}^{+\infty} \frac{dy\, e^{-y^2}}{x+y+ib}$$

$$x = (4\ln 2)^{1/2} \frac{\nu_0 - \nu}{\delta \nu_D},$$

$$b = (4\ln 2)^{1/2} \frac{\delta \nu_0}{\delta \nu_D}.$$

Eq. 12

$\delta\nu_D$ is the FWHM Doppler broadening width, and $\delta\nu_0$ is the sum of the natural linewidth and the collision broaden linewidth.

If the optical pumping saturates the population difference, then the population density n_M at steady state is approximately,

$$n_M = \frac{N_{J''}}{2J''+1} \frac{1}{1 + \dfrac{I_p \sigma_M{}^P(\nu_p)}{h\nu R}} \quad ,$$

Eq. 13

where $N_{J''}$ is the unsaturated total population of the rotation level J", Ip is the intensity of the saturating pump, $\sigma_M{}^P(\nu_p)$ is the absorption cross-section for the circularly polarized pump beam at pumping transition frequency ν_p, and can be calculated using Eq. 9. R is the relaxation rate that will refill the energy level (J",M"). Because $\sigma_M{}^P$ is different for each M, the optical pumping will result in a population difference among the magnetic sublevels. This, in turn, creates the different refractive indices for the right-handed and left-handed polarizations, and hence produces the optical polarization rotation. Fig. 5 illustrates an absorption cross-section σ^+ that is M dependent (assuming M=88).
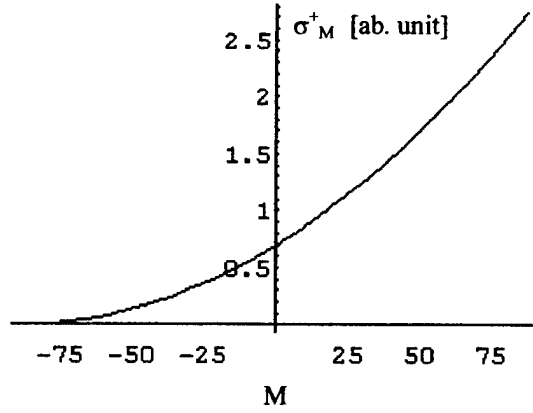
Fig. 5. An illustration of the absorption cross-section M dependence for a right-handed circular polarized light.

Molecular ro-vibrational energy levels are easily depleted by laser excitation compared with atomic energy levels, because, unlike spontaneous emission in atoms in which most of the energy radiates back to the initial ground state, in molecules there are very large number of ro-vibrational energy levels in the ground state and the emitted photons rarely return to the molecules to the same initial state. Thus the dominant relaxation process that refills a depleted energy level is through collision relaxation of the ro-vibrational energy states. This process is usually very slow compared with the rate of depopulation by laser pumping. Therefore, the dominant relaxation process is due to collisions. The relaxation rate can be calculated by,

$$R = \sigma_c N_0 \bar{v} \qquad , \qquad \text{Eq. 14}$$

where σ_c is the collision cross-section, N_0 is the total number density, and $\bar{v}$ is the molecular average thermal velocity.

Once the absorption coefficients and refractive indices are known, then the filter transmission can be calculated. The filter design parameters, the pump intensity, the molecular density and vapor cell length, can be determined through the process of optimizing the transmission for different operating conditions.

To compare the LIDOF performance, we define the total equivalent noise bandwidth (ENBW) for the filter as

$$ENBW = \frac{1}{T_{max}} \int_{-\infty}^{+\infty} T(\omega) \, d\omega \qquad \text{Eq. 15}$$

where $T(\omega)$ represents the filter transmission spectrum and T_{max} represents the maximum transmission for the filter. The equivalent noise bandwidth corresponds to the bandwidth of a rectangular notch filter with transmission T_{max} that transmits the same amount of the noise as our filter. Using the ENBW, we can easily compare different filter designs and

10

performance. If the noise power spectrum is about constant within the bandwidth of the filter, the noise rejection factor (NRF) may be calculated as

$$NRF = \frac{(Total\,incident\,noise)T_{max}}{Total\,noise\,transmitted}$$

Eq. 16

$$\approx \frac{\int_0^\infty p_n(\lambda)\cdot d\lambda}{p_n(\lambda_0)\cdot ENBW}$$

where $p_n(\lambda)$ represents the solar radiation power spectrum, or solar radiation spectrum, λ_0 is the center wavelength of the filter. The approximation in the NRF equation is valid if $p_n(\lambda)$ is approximately constant within the filter bandwidth. This is true for most narrow bandwidth filters. To simplify the NRF calculations, the solar noise power spectrum at sea level may be modeled as a blackbody radiation at 5770 °K.

The optimized operating conditions for the Na_2 vapor 532 nm LIDOF are calculated to be optical pump of 500 W/cm^2 and a cell temperature of 600 °C for the standard commercial cell length of 25 cm. The calculated transmission spectrum is shown in Fig. 6.
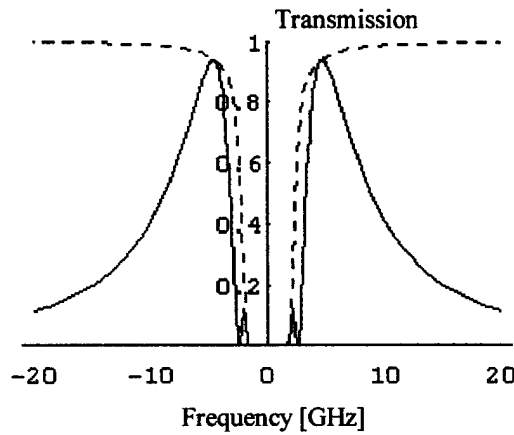

Fig. 6. The transmission spectrum of the Na₂ LIDOF at 532-nm (solid line) and transmission spectrum of a Na₂ cell at 532-nm (dashed line).

In Fig. 6, the horizontal axis is frequency in giga-hertz, where 0 Hz is the center of the absorption line. Fig. 6 shows that the transmission peaks are just outside resonance absorption. The peak transmission is calculated to be about 93%, with bandwidth about 5 GHz. The equivalent noise bandwidth (ENBW) is calculated to be 16 Ghz. The noise rejection factor is about 50 dB. Fig. 7 is the calculated rotation angle versus frequency at the same operating conditions.
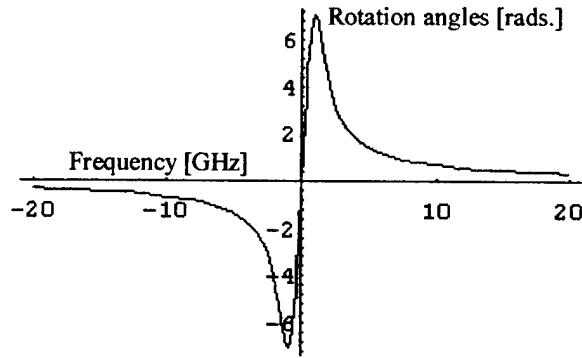
Fig. 7. The calculated rotation angles for linearly polarized light passing through the vapor cell.

Fig. 7 clearly shows that large rotation angles may be obtained near the resonance line center. Fig. 8 shows the calculated population density distribution versus the sublevel quantum number M" of the level J" (J"=23) in ground state.
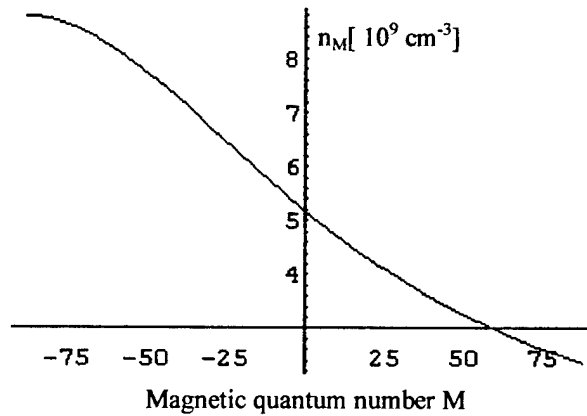

Fig. 8. The population density n_M [$10^9/cm^3$] versus quantum number M" of the level J"=88, v''=1.

Fig. 8 illustrates that optical pumping by a circularly polarized pump results in a significant population difference among the M" sublevels of the J" ground state, which results in an optical polarization rotation.

The LIDOF peak transmission is dependent on the molecular number density, the pump power, and cell length. The cell temperature will determine the molecular number density. The pumping creates the non-equilibrium and polarized population distribution that generates the optical rotations and the collisions tend to restore the equilibrium population distribution. Fig. 9 shows the peak transmission of the LIDOF versus the pump power at three different cell temperatures (or total molecular number densities) for an Na_2 510 nm LIDOF.
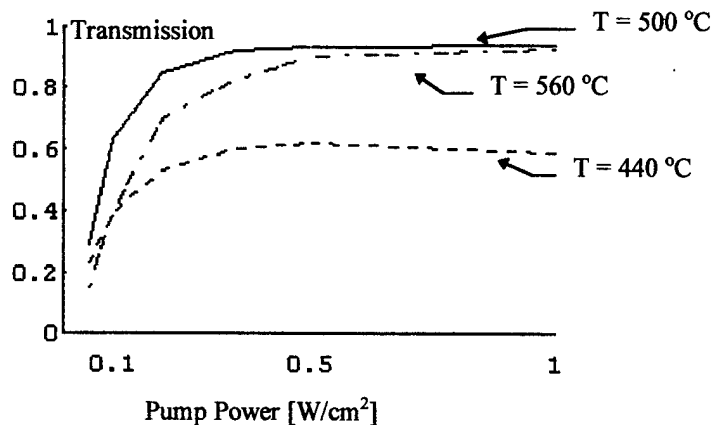
Fig. 9. 532 nm LIDOF (cell length 25 cm) peak transmission versus pump power.

The peak transmission is restrained by the pump power and by the molecular density. Larger rotation angles require sufficient molecular number density and pump power. When the molecular number density is increased, the molecular collision rate also increases. This decreases the rotation angles. Therefore, to increase the rotation angles, the laser pump power must be increased by an appropriate amount. The maximum available number density is determined by the practical cell temperature and by the maximum available pump power. The optimum operating conditions are chosen by appropriate balancing the requirement for cell temperature, pump power, and collision rate that we will discuss later.

An alternative way to increase the throughput is to increase the cell length. Fig. 10 shows the 532 nm Na_2 LIDOF peak transmission versus the cell length at cell temperature of 600 °C and pump intensity of 500 W/cm^2.
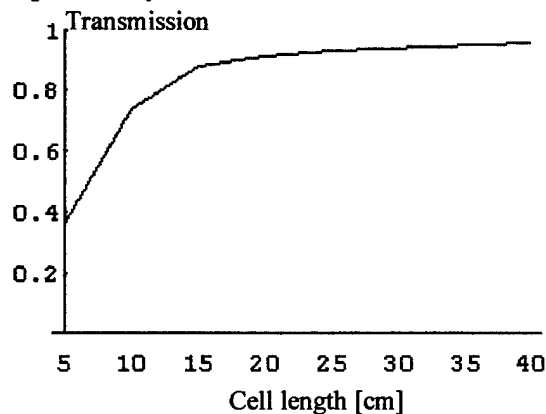

Fig. 10. The peak transmission vs. the cell length at the temperature of 600 °C and optical pump of 500 W/cm^2.

Although the longer the cell length, the higher the throughput, the cell length is limited by the field of view considerations.

As we mentioned early, the dominant relaxation process for a molecular rotation level is through collision. For the Na_2 532 nm LIDOF, the cell temperature is about 600 °C, where the total number density for Na_2 molecules is about 2×10^{15} cm^{-3} and the total number density for the Na atoms is about 25 times higher. The collision cross-section for Na_2 molecule is about 10^{-14} cm^2 [19]. Therefore, the total collision rate, R, for the Na_2 532 nm LIDOF is about 4.2×10^7 s^{-1} at 600 °C cell temperature, which corresponds to a relaxation time of about 25 ns. In other words, a 50% non-equilibrium population generated by optical pumping will be destroyed by collisions in 25 ns after the end of the optical pump pulse. Once the non-equilibrium population is gone, there will be no dispersion in the molecular vapor cell, which means no light will be transmitted through the crossed polarizers of the filter. Therefore, the optical pumping will provide an ideal gating system for the receiver. In this gating system, the laser pumping is synchronized with return beacon signal pulse. The laser pumping pulse length is controlled to be about the same length as the signal pulse length. The risetime of this laser activated gating system is about 25 ns for 532 nm Na_2 LIDOF. Therefore, the maximum energy required for the pump laser pulse is determined by the signal pulse length.

Table IV summarized the parameters and performance of the Na_2 532 nm LIDOF.

Table IV. Summary of the Na_2 532 nm LIDOF

signal wavelength: 532 nm
signal transition: B-X(10,3) P127
pump wavelength: 728.0 nm
B-X lifetime: 6.5 ns
signal absorption crossection: 1×10^{-16} cm^2
pump absorption crossection: 0.9×10^{-15} cm^2
cell length: 25 cm
cell temperature: 500 °C
collision crossection: 10^{-14} cm^2
collision rate: 4.2×10^7 s^{-1}
pump intensity: 500 W/cm^2
peak transmission: 0.8
transmission bandwidth: 5 GHz
equivalent noise bandwidth (ENBW): 16 GHz
solar noise rejection factor: 10^5
gating risetime: 25 ns

3) Experimental System Design

The major components to building a Na_2 532 nm LIDOF are a heat pipe oven for the Na_2 vapor, a laser pump to polarize the Na_2 molecules, and a laser signal source to test the filter performance. A basic overview of the experimental system is shown in Fig. 11.
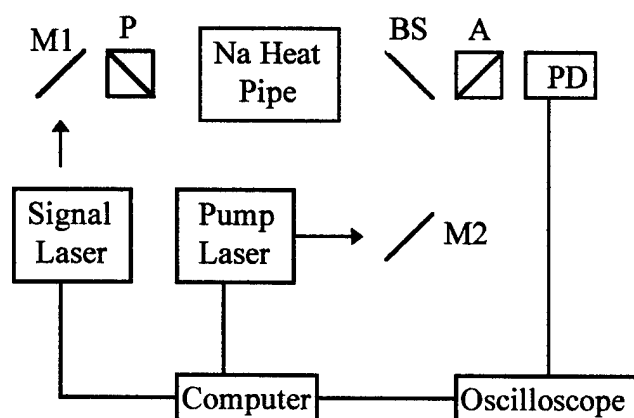

Fig. 11. LIDOF experimental system block diagram. M1 and M2 represents mirrors. P and A represent the polarizer and analyzer pair. BS represents a dichoric beam splitter. PD represents the photo-detector.

The Na_2 molecules are a narrow bandwidth birefringent medium when they are pumped by a narrow bandwidth circularly polarized pump source tuned to one specific molecular transition. The heat pipe ensures that the proper Na_2 vapor density is maintained. The crossed polarizers ensure that only radiation whose polarization has been rotated by the polarized Na_2 molecules reaches the photo-detector. The signal laser is a narrow bandwidth test oscillator that is tuned to filter transmission band.

The pump laser radiation is reflected off mirror M2 and the dichoric beam splitter BS and travels through the heat pipe to the left. Meanwhile the signal radiation is reflected off the mirror M1, and directed into the polarizer P, travels through the heat pipe, and is transmitted through the dichoric beam splitter BS. If the signal radiation frequency is tuned to the filter passband, then the signal radiation is polarization rotated by $\pi/2$ and is transmitted through the analyzer A with high efficiency. If the signal radiation is not tuned to the filter passband frequency, then the radiation is extinguished by the analyzer. In the next few sections we will discuss each element of the experimental system in detail.

(A) Na_2 vapor oven

The heart of the LIDOF is the Na heat pipe. This device is commercially available and can operate up to temperatures of 700 °C with standard vapor zones of up to 25 cm long. For our experiments we do not expect to operate at temperatures above 600 °C; thus

the heat pipe technology is sufficient. The heat pipe technology used for the Na_2 LIDOF is the same type of system that has proved successful for all of alkali-dimer lasers [20]. Because of the relatively low vapor pressure of the Na_2 molecule, an operating temperature of 500 °C is necessary to generate a sufficient density of Na_2 molecules for efficient LIDOF operation. The easiest means of operating at these temperatures is in a heat pipe because only the metal comes in contact with the high temperatures and the windows can be maintained at room temperature. Heat pipes are back filled with a rare gas. The rare gas is forced out of the hot regions as the metal vapor pressure increases. Thus, only the rare gas comes in contact with the windows. This is a significant advantage because it eliminates any chemical compatibility problems that could occur if the glass were in direct contact with hot metal at high temperatures. The modern heat-pipe oven has continuously generated homogeneous pure metal vapors of well defined pressure, temperature, and optical path length. All parameters can be measured easily and accurately. The simplified schematic diagram of a heat-pipe oven is shown in Fig. 12.
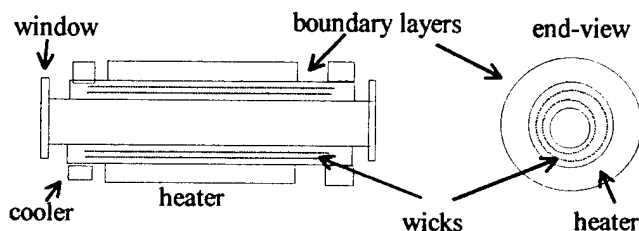

Fig. 12 The simplified schematic diagram of the heat-pipe oven.

The heat-pipe is made of stainless steel. The outer wick of the inner tube and the wick of the outer heat-pipe are both made out of a few layers of stainless steel mesh. The inner and outer wicks are connected to provide a path back to the outer wick to avoid accumulation of the vapor material on the inner wick. Also, a suitable amount of an inert gas will be put inside the tube. This will confine the alkali metal to vapor section and will keep the windows clean. According to the Na_2 LIDOF operating conditions, the heat-pipe will be operated at 600 °C and a vapor length of 25 cm. Because the LIDOF is not sensitive to small temperature change or small vapor length change, no special effort is needed to control the cell temperature and vapor length. We purchased a Na heat-pipe from Comstock Corporation. Heat pipes are generally operated at less than atmospheric pressure and are back filled with several torr of a rare gas. The heat pipe was tested up to 650 °C and performed well.

(B) The Pump Laser

The pump laser is a Candela flash lamp pumped dye laser modified to produce 2 GHz wide pump lines with 3.6 mj output energy with the flashlamp voltage set to 23 kV. The laser linewidth was measured to be 0.07 cm^{-1} when the laser was operated at 1 Hz. the linewidth increased to 0.072 cm^{-1} when the laser was operated at 2 Hz. We also measured the jitter in the position of the pump laser line and that was measured to be 0.01 cm^{-1}. The

laser linewidth and line center wavelength were measured using a Burleigh wavemeter and averaged over 25 pulses. The LIDOF temporal response follows the pump pulse. The easiest method for varying the pump pulse duration is to use a cw pump laser and electro-opitcally turn the pulse on or off. The power levels that are needed can easily be delivered by commercial cw dye lasers

4) Conclusions:

We modeled and delivered a Na FADOF with high throughput and ultra-high background rejection at 589-nm. Furthermore, we modeled, designed, and delivered a novel optical filter for 532-nm, the LIDOF. The LIDOF is waiting to be tested at the laser wavelength. All that remains to be done in future work is to obtain a test oscillator at 532 nm and to perform the final tests.

REFERENCES:

1)   D. J. Dick and T. M. Shay, "Ultra-high noise rejection optical filter," Opt. Lett.16, p. 867(June 1991).

2)   B. Yin and T. M. Shay, "Theoretical model of Faraday anomalous dispersion optical filter," Opt. Lett. 16, p. 1617-1619 (Oct. 1991).

3)   B. Yin and T. M. Shay, "A potassium Faraday anomalous dispersion optical filter," Optics Communications, vol. 94, p. 30-32 (Nov. 1992).

4)   B. Yin and T. M. Shay, "Faraday anomalous dispersion optical filter of Cs 455 nm," IEEE Photonics Technology Lett., vol. 4, p.4 88-490 (May 1992), addendum to this article, IEEE Photonics Technology Lett., vol. 5, issue 4 (April 1993).

5)   T. M. Shay and B. Yin, "Faraday anomalous dispersion optical filter, Proceedings of the International Conference on Lasers '91, p. 641-648, San Diego, CA (Dec. 1991).

6)   B. Yin and T. M. Shay, "Faraday anomalous dispersion optical filter of potassium," Proceedings of the SPIE OE'Laser '92, 641-648, Los Angeles, CA (Jan. 1992).

7)   T. M. Shay, B. Yin, and L. S. Alvarez, "Faraday anomalous dispersion optical filter," International Conference on Lasers '92, 829-836, Houston, TX (Dec. 1992).

8)   B. Yin and T. M. Shay, "Theoretical model for a novel ultrahigh optical background rejection optical filter," XVIII International Quantum Electronics Conference, Vienna, Austria (June 1992).

17

9)   T. M. Shay and B. Yin, "Theoretical model for a Faraday anomalous dispersion optical filter operating at Ca 423-nm," IEEE Laser and Electro-Optics Society Annual Meeting, Boston, MA (Nov. 1990).

10) A. M. Title and W. J. Rosenberg, "Improvements in birefringent filters," Appl. Optic. 18, p. 3443-3456 (Oct. 1979).

11) T. M. Shay and Y. C. Chung, "An ultra-high resolution, wide field-of-view optical filter for doubled Nd:YAG," Optics Lett. Vol. 13, p. 443 (June 1988).

12) T. M. Shay and D. Garcia, "Theoretical Model for a background noise limited Rb laser-excited optical filter for doubled Nd lasers," IEEE J. Quantum Electro., Vol 26, p. 1135 (June 1990).

13) M. Minden, H. Bruesselbach, "Detection of 532-nm frequency-doubled Nd:YAG radiation in an active rubidium atomic resonance filter," Optics Lett. Vol. 15, No. 7, p. 384 (April 1990).

14) J. A. Gelbwachs, "Atomic resonance filters," IEEE J. Quant. Electr. 24, p. 1266 (July 1988).

15) A. F. Molisch, B. P. Oehry, W. Schupita, and G. Magerl, "Quantum efficiency and signal bandwidth of thallium atomic line filters," Opt. Comm. 90, p. 245-250 (June 1992).

16) B. Yin, L. Alvarez, and T. Shay, "The Rb 780 nm Faraday anomalous dispersion optical filter," NASA/JPL TDA Report, 42-116, p. 71-85 (Feb. 1994).

17) J. Menders, K. Benson, S. Loom, C. Liu, and K. Korevaar, "Ultranarrow line filtering using a Cs Faraday filter at 852-nm," Opt. Lett. 16, p. 846 (1991).

18) M. Abramowitz and I. A. Stegun, Handbook of Mathematical Functions, Dove, New York, p325-328 (1971).

19) W. Demtroder, Laser Spectroscopy, Springer-Verlag, New York, p.595 (1981).

20) B. Wellegehausen, "Optically Pumped CW Dimer Lasers," IEEE Journal of Quantum Electronics, Vol. QE-15, n0, 10, 1108, (1979).

AUL/LSE
Bldg 1405 - 600 Chennault Circle
Maxwell AFB, AL 36112-6424   1 cy

DTIC/OCP
8725 John J. Kingman Rd, Suite 0944
Ft Belvoir, VA 22060-6218   2 cys

AFSAA/SAI
1580 Air Force Pentagon
Washington, DC 20330-1580   1 cy

AFRL/PSTL
Kirtland AFB, NM 87117-5776   2 cys

AFRL/PSTP
Kirtland AFB, NM 87117-5776   1 cy

Shay Aerospace Corporation
1300-G El Paseo, Suite 304
Las Cruces, NM, 88001   1 cy

AFRL/DE/Dr Hogge
Kirtland AFB, NM 87117-5776   1 cy

Official Record Copy
   AFRL/DES/Dr. Paul Hillman   5 cys